A study of black aurora from aircraft-based optical observations and plasma measurements on FAST

L. M. Peticolas
Space Sciences Laboratory, University of California, Berkeley, California, USA

T. J. Hallinan and H. C. Stenbaek-Nielsen
Geophysical Institute, University of Alaska, Fairbanks, Alaska, USA

J. W. Bonnell and C. W. Carlson
Space Sciences Laboratory, University of California, Berkeley, California, USA

Received 6 July 2001; revised 5 October 2001; accepted 5 October 2001; published 29 August 2002.

[1] Black aurora was observed on 30 January 1998 in a narrow-field camera forty seconds before and a minute after the magnetic footprint of the FAST satellite passed the magnetic zenith of the camera. Electron energy flux measured by FAST provided strong evidence that FAST passed over black aurora. This region was characterized by small-amplitude wave and DC electric fields (<10 mV m^{-1}) and small upward current densities ($\sim$0.2μA m^{-2}). The electron energy flux dropouts associated with black aurora were associated with spatially restricted regions in which the strong pitch angle diffusion is suppressed at energies greater than $\sim$2 keV. These dropouts were surrounded by hot ($\sim$1.8 keV) plasma sheet electrons exhibiting strong pitch angle diffusion at all measured energies. Analyzing the electron spectra from six different nights of optical and satellite conjugate data demonstrates a surprising prevalence of electron distributions that showed the suppression of strong pitch angle diffusion at energies above $\sim$2 keV. What made the electron signature on the night of the black aurora observations unique were the large spatial regions of strong pitch angle diffusion at all energies (corresponding to the diffuse aurora) with only very narrow spatial regions of the partially empty loss cones (corresponding to the black aurora). We suggest that the pitch angle diffusion surrounding the black aurora is due to electron cyclotron waves (ECH) strongly scattering electrons into the loss cone at energies less than $\sim$2 keV and oblique, upper band whistler mode chorus waves scattering electrons at all measured energies in the plasma sheet. We further suggest that the scattering by the chorus waves is suppressed in localized regions leading to the black auroral features observed. *INDEX TERMS:* 2704 Magnetospheric Physics: Auroral phenomena (2407); 2716 Magnetospheric Physics: Energetic particles, precipitating; 2720 Magnetospheric Physics: Energetic particles, trapped; *KEYWORDS:* black aurora, diffuse aurora, electron precipitation, whistler mode chorus, auroral satellite, electron anisotropy

1. Introduction

[2] Black aurora is defined as the absence of auroral emissions in well-defined regions within a uniform background of emission [*Royrivik*, 1976; *Davis*, 1978]. These dark regions have been observed as several distinct forms: black patches, black rings, black arc segments, thin black arcs, and black vortex streets (black curls) [*Oguti*, 1975; *Royrivik*, 1976; *Davis*, 1978; *Schoute-Vanneck et al.*, 1990; *Trondsen and Cogger*, 1997; *Kimball and Hallinan*, 1998a, 1998b]. Black auroral forms are small-scale features with widths (or minor axes) ranging from 100 m to 5 km [*Trondsen and Cogger*, 1997; *Kimball and Hallinan*, 1998a, 1998b]. Black patches and rings have major axes ranging from 2 to 14 km and arc segments have lengths on the order of 20–30 km. Black arcs and vortex streets do not have well-defined lengths since they are longer than the fields of view of low-light auroral TV cameras used to date (>40 km) [*Trondsen and Cogger*, 1997; *Kimball and Hallinan*, 1998b]. All types of black aurora have typical drift speeds near 1 km s^{-1} [*Kimball and Hallinan*, 1998a, 1998b].

[3] Black arcs will often twist in a clockwise direction, forming black vortex streets (black curls). Although rare, black curls have been observed intertwined with white curls [*Kimball and Hallinan*, 1998a]. These white curls are similar to black curls in their horizontal drift speed relative to the star field ($\sim$0.6 km s^{-1}) and also similar in the wavelength ($\sim$2.4 km) of their vortices but twist in the counterclockwise direction. Black curls are most frequently observed in the midnight sector, as are the other types of black aurora. Black curls have never been observed in conjunction with

Copyright 2002 by the American Geophysical Union.
0148-0227/02/2001JA900157$09.00

pulsating aurora whereas other types of black auroral forms are sometimes colocated with pulsating aurora [*Trondsen and Cogger*, 1997; *Kimball and Hallinan*, 1998a, 1998b]. Additionally, black curls have been observed to drift horizontally both eastward and westward within the diffuse aurora, whereas black patches and rings always drift horizontally eastward unless moving around a pulsating auroral patch [*Trondsen and Cogger*, 1997; *Kimball and Hallinan*, 1998b].

[4] The theory of black curls is the only well-developed theory of black aurora. *Royrivik* [1976] first suggested that black curls were related to excess positive space charge, analogous to discrete white arc curls associated with excess negative space charge [*Hallinan and Davis*, 1970; *Trondsen and Cogger*, 1998; *Vogt et al.*, 1999]. *Marklund et al.* [1994] proposed that the narrow diverging electric fields, dropouts of precipitating electrons, depletions of thermal plasma, and significant wave activity observed in data from instruments on-board the Freja satellite were indications of positive space charge and thus, black curls. After these observations, *Johnson and Chang* [1995] have shown that two-dimensional solitary nonlinear plasma waves can have characteristics consistent with the Freja observations. *Keskinen and Ganguli* [1996] have simulated the nonlinear evolution of the stratified Kelvin-Helmholtz shear instability and reproduced both the Freja signatures and the time evolution seen in optical observations of black curls. *Kimball and Hallinan* [1998a, 1998b] used the similarity of black curls and discrete arc curls to derive electric field strengths from optical measurements of black curls, finding electric fields consistent with the Freja measurements.

[5] Even with the wealth of models, optical data, satellite and rocket data, presently no conjugate optical and in situ measurements of black aurora have been reported. However, on 30 January 1998 black aurora was observed in a narrow field camera forty seconds before and a minute after the footprint of FAST passed the zenith of the narrow-field camera allowing for a detailed examination of the plasma environment in which black aurora is found. In this paper, we begin with an overview of the optical observations from the TV camera data and of the plasma environment from instruments on the FAST satellite. Next, we show evidence that FAST passed over black aurora using high time resolution electron energy fluxes and narrow-field camera observations. The electron signatures that produce dropouts in energy flux indicative of black aurora and the flux surrounding the dropouts are then studied in detail. In order to ascertain the uniqueness of the electron spectra on the night of the black aurora, the electron spectra measured on six additional nights in which black aurora was not observed are then studied. A discussion on the data and its implications on previous black auroral research is presented at the end of the paper.

2. Instrumentation

[6] A Sabre-60 jet aircraft was instrumented with low-light intensified TV cameras for two campaigns to observe aurora conjugate to the FAST satellite [*Stenbaek-Nielsen et al.*, 1998]. Observations around 29 conjunctions in the late evening sector (20–22 MLT) were made during the months of January and February of 1997 and 1998.

[7] The low-light level TV cameras used to make the optical observations in the 1998 campaign consisted of an all-sky camera and two narrow-field cameras. The narrow-field cameras were silicon intensified target (SIT) cameras having $29^\circ \times 22^\circ$ fields of view. All three cameras were mounted to look up through windows in the ceiling of the aircraft with one narrow-field camera pointing in the direction of the magnetic zenith. The narrow-field cameras were fitted with a notch filter to eliminate the atomic oxygen, O I 5577 Å line emission.

[8] Electrostatic analyzers on board FAST provided full electron and ion distribution functions across the auroral oval every 0.83 or 0.64 s, depending on the instrument mode for a particular oval crossing. During short periods of time, data were collected in a burst mode, giving full electron and ion distribution functions every 0.079 s. Electron differential energy fluxes are sampled at 48 energies (4 eV to 32 keV) and 32 pitch angles (0–360°). Ion differential energy fluxes had the same angle sampling array, but an energy sampling array of 48 energies from 3 eV to 25 keV [*Carlson et al.*, 2001]. Dual baseline boom pairs measured vector DC electric fields in the range ±1.6 V/m from 0–1 kHz (in survey mode) [*Ergun et al.*, 2001]. A flux gate magnetometer measured DC magnetic fields in the range $\pm 6 \times 10^4$ nT from 0 to 10 Hz [*Elphic et al.*, 2001].

3. Data Overview

3.1. TV Camera Observations

[9] In order to calculate the horizontal spatial scales and drift speeds of black aurora observed with the optical TV cameras, one must know the height of the auroral emission surrounding the black aurora. An estimate of this height was made using the FAST electron data with a 16-stream electron transport calculation [*Lummerzheim and Lilensten*, 1994]. The upper boundary condition for the transport code was obtained by mapping the electron differential number flux adjacent to the region in which black aurora was embedded (the flux in the region C in Figure 2, discussed below) from FAST altitudes (~4000 km) down to 400 km using Liouville's theorem. The transport code used MSIS90 [*Hedin*, 1991] as a neutral atmospheric model. The altitude of the peak energy deposition adjacent to the black aurora was calculated to be 115 km, which was then used to obtain the widths and drifts of the optical black aurora in this section.

[10] Prior to the aircraft conjunction (0850:11 UT) with FAST on 30 January the aurora had been continuously active for several hours, with at least three westward traveling surges or other activations. From 0847:19 UT to 0947:33 UT, black aurora was observed sporadically in the airborne-based TV cameras in the form of black arcs, arc segments, and black curls. The black forms were located poleward of pulsating aurora and equatorward of discrete auroral arcs, were seen in association with white curls, and occurred in relatively bright diffuse aurora that changed in time to discrete aurora and then back to diffuse aurora. These features are all in agreement with past observations of black aurora [*Oguti*, 1975; *Schoute-Vanneck et al.*, 1990; *Trondsen and Cogger*, 1997; *Kimball and Hallinan*, 1998a].

[11] As FAST passed into view of the all-sky camera (0847:32 UT), there were still active, bright auroral discrete arcs to the northeast and the southwest of the aircraft, as

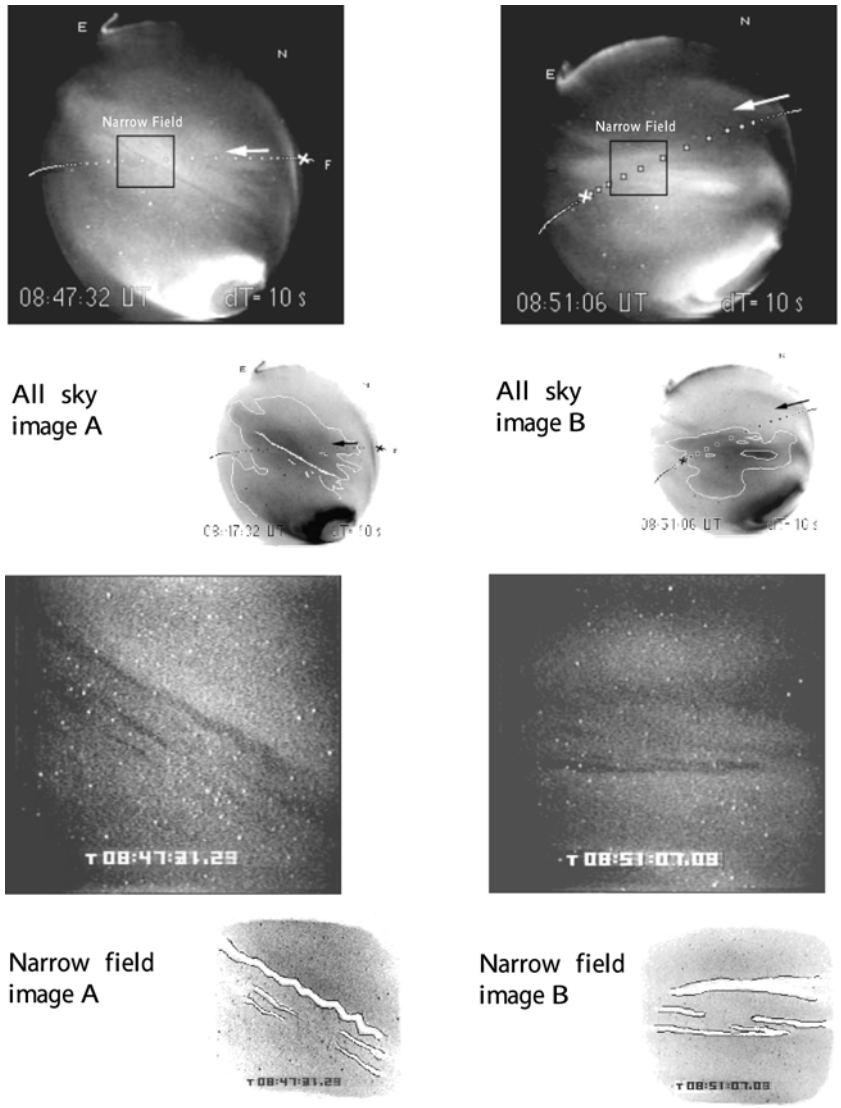

Figure 1. Black aurora seen in the narrow-field cameras and the associated all-sky images before and after conjunction with FAST.

shown in all-sky image A in Figure 1, where the inverse of the original image is shown beneath the original image with sketches to emphasize features in the original images.

[12] The dots across the all-sky images in Figure 1 represent the footprint of the FAST satellite at 100 km every 10 s, the small cross shows the location of FAST at the times marked in the lower left corner of the images, and the arrow represents the direction of the projected velocity of FAST.

[13] A black auroral arc with a width of 6.5 km was observed above the aircraft in diffuse aurora at 0847:32 UT as shown in Figure 1, All-sky image A. The image taken from the narrow-field camera (Figure 1, narrow-field image A) shows that this black arc is curled in the clockwise direction and is present near smaller black arc segments. These arcs drifted to the southeast with a speed of 1.1 km s^{-1}. As the magnetic footprint of FAST approached the zenith, the diffuse aurora changed shape into a thick arc, brightening until conjunction (0850:11 UT) at which time the arc contained discrete auroral forms. After FAST passed overhead the arc then changed back to a dimmer, more diffuse arc with embedded black auroral arc segments (0851:07 UT), shown in the right column of Figure 1. These arc segments drifted to the southeast with a speed of 1.7 km s^{-1} and increased ~50% in width as they drifted. The drift speeds and dimensions of the black auroral forms seen this night are typical of drift speeds associated with black aurora as discussed above. Soon after conjunction, there was a substorm onset at 0900 UT.

3.2. FAST Observations

[14] The accelerated electron spectra measured by instruments on the FAST satellite on 30 January 1998 (orbit 5700) were not especially energetic, but the plasma sheet electrons often associated with diffuse aurora were especially hot with a temperature of ~1.8 keV. In Figure 2 (top panel), the plasma sheet electron spectra within the precipitating loss cone (0 ± 28°) can be seen to have significant differential energy flux up to 10 keV in some places and overlaps regions of ''inverted-V'' electron spectra.

[15] The upgoing energy spectra of electrons with pitch angles of 180 ± 22° are shown in Figure 2 (second panel). Note that there are large differential energy fluxes of low-

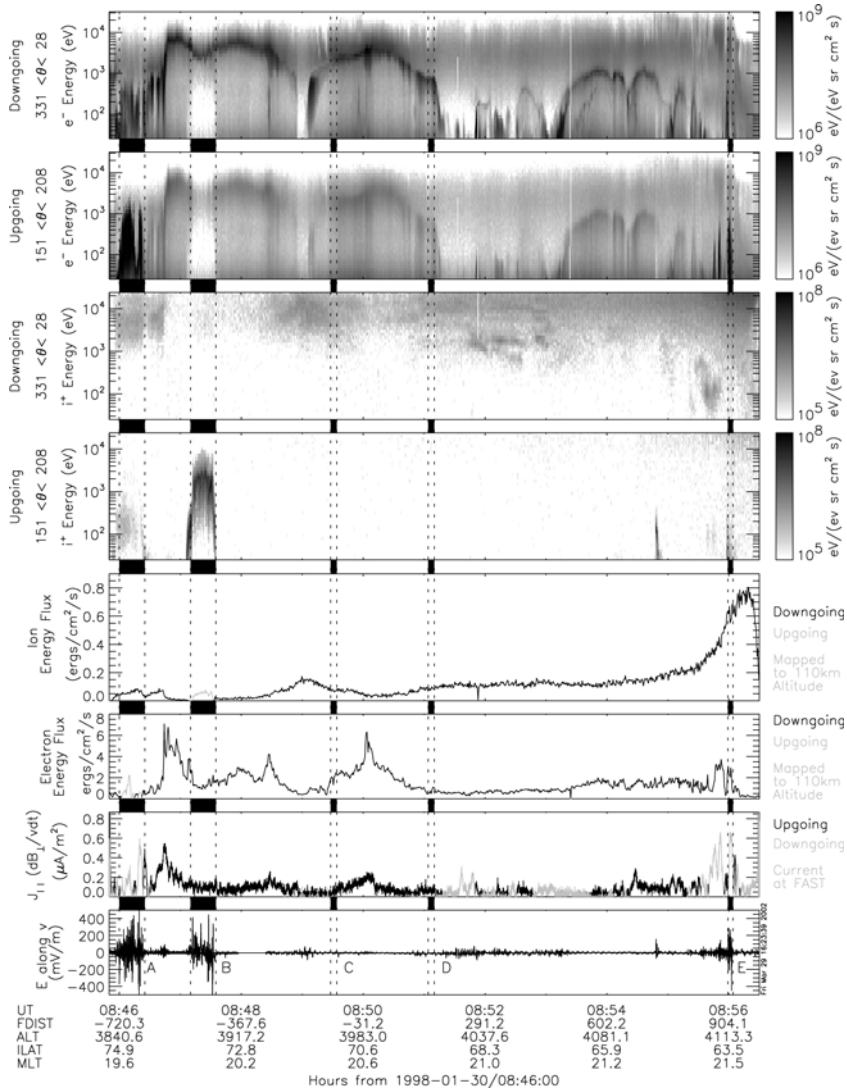

Figure 2. Particle and field measurements for FAST orbit 5700. See text for details. See color version of this figure at back of this issue.

energy, upgoing electrons only at the poleward and equatorward boundaries of the auroral oval.

[16] When comparing the FAST electron data shown in Figure 2 (top two panels) with the optical data, it is important to keep in mind that the aurora was changing, albeit slowly, while FAST crossed the auroral oval. The footprint of FAST crossed the magnetic zenith of the narrow-field camera at 0850:11 UT when there was an accelerated (inverted-V) spectrum (Figure 2, top panel) and the aurora was relatively bright. However, at that same location in the ionosphere 40 s before (at 0849:30 UT) and a minute afterward (at 0851:07 UT), the aurora was dimmer and more diffuse with black auroral forms. The diffuse aurora covered a large portion of the sky including the area where the footprints of FAST were located. The black aurora observed at 0851:07 UT in the magnetic zenith and the location of the footprint of FAST are shown in the images in Figure 1, right column. From the all-sky images we conclude that the electron spectra measured around the times 0849:30 and 0851:07 UT, far from the magnetic zenith is similar to that which caused the diffuse aurora in the magnetic zenith. These differential energy fluxes are the result of a small acceleration causing a small but visible integrated energy flux.

[17] The downgoing ions with pitch angles of 0 ± 28° during this night had very large differential energy fluxes at high energies, especially near the equatorward edge of the auroral oval (Figure 2, third panel). Two up-going (180 ± 28°) ion beams were measured and are shown in Figure 2 (fourth panel) in regions B and E at 0846:45 and 0855:00 UT, respectively. The downward ion pitch angle integrated energy flux was the largest of all seven nights studied, peaking at 0.8 erg cm^{-2} s^{-1} at the equatorward edge of the oval (Figure 2, fifth panel).

[18] The pitch angle integrated energy fluxes in Figure 2 (fifth and sixth panels) were obtained by first integrating the precipitating loss cone (source cone) differential energy flux, then subtracting from this quantity the integrated upward loss cone differential energy flux, and lastly mapping the resulting energy flux to 110 km. When the net energy flux is downgoing, the flux is color coded green. For cases when the upgoing energy flux is larger than the

downgoing energy flux, the resulting negative energy flux is plotted as a positive value, color coded in red. Often, the upward energy flux is small, consisting mostly of backscattered electrons. In such cases the net energy flux represents the energy flux that is absorbed by the upper atmosphere, leading to ionizations and excitations of the atmospheric species. When the measured electron energy flux leaving the ionosphere is large, the process causing the significant upward electron flux, e.g. a downward parallel electric field, will affect the downward flux. The net energy flux accounts for this effect by decreasing the downward energy flux or producing a net upward energy flux in such cases.

[19] For slowly varying (>1 s) auroral electron fluxes, the above calculation of precipitating energy flux best represents the brightness observed by the all-sky camera without performing a detailed transport calculation. The aurora we studied for this manuscript did vary sufficiently slowly and the electron energy flux in Figure 2 (sixth panel) agrees with the variation in the optical signal observed with the TV cameras. These cameras typically resolve electron energy fluxes of $\sim$1 erg cm^{-2} s^{-1} and higher. There is also good agreement between the changes in the energy deposition rate calculated from the transport code, as discussed above, and the electron energy fluxes.

[20] The parallel current density was estimated from the changes in the cross-track component of the perturbation magnetic field and the spacecraft velocity perpendicular to B_o. This current is shown in Figure 2 (seventh panel). At the poleward boundary of the auroral oval (0846:00 UT, Region A) the currents are downward with a strong flux of upward traveling electrons. From 0846:40 UT until 0851:20 UT, the currents are upward, the typical direction of currents associated with inverted-V electron spectra. Figure 2 shows that in the diffuse aurora (0851:00–0855:30 UT) and in the region of black aurora (regions C and D) the current densities are very small ($\sim$0.2 μA m^{-2}). At the equatorward boundary of the auroral oval (0855:30–0856:30 UT, near region E), the currents are more structured with upward and downward directed electron beams.

[21] The electric fields measured by FAST are shown in Figure 2 (eighth panel). Spikes in the estimated electric field due to spin-periodic solar and magnetic shadowing of the electric field probes have been removed from the data. The electric field data have been interpolated through these times. As can be seen, the electric fields at FAST ($\sim$4000 km altitude for this study) are all less than 400 mV m^{-1}. On both the poleward edge and equatorward edge of the auroral oval, in the regions marked A and E, are some of the largest measured electric fields (>200 mV m^{-1}). These electric fields are made up of solitary waves coincident with VLF emissions like those described by *Ergun et al.* [1998]. Both of these boundaries are associated with downward current regions and upward electron beams. At 0847:10–0847:40 UT, region B, there are also large electric fields in the middle of an inverted-V structure concurrent with an upward ion beam. These fields are primarily diverging and converging perpendicular fields with a total integrated potential over the time of the ion beam of 4 keV. Region B is a typical example of the plasma and fields signatures when FAST flies through the acceleration region [e.g., *Ergun et al.*, 2000]. Small-amplitude (<10 mV m^{-1}) wave electric fields with frequencies around 130 Hz were measured in the diffuse arc region where FAST passed through black aurora, marked as regions C and D. There was also auroral kilometric radiation (AKR) measured continuously from $\sim$0845 to 0852 UT. There were no unusual wave spectra near or in the black aurora regions. All of these types of electric fields and particle signatures are commonly observed at FAST altitudes in the auroral oval [*McFadden et al.*, 1999, and references therein] and were seen in all of the six other conjugate data nights included in this study.

4. Electron Signatures of Black Aurora

[22] Even though FAST crossed black aurora signatures at the same time as black aurora was observed in the magnetic zenith (0851:07 UT), because FAST was out of the magnetic zenith, the black arcs in the narrow-field image B in Figure 1 are not the same as those sampled at FAST at this time. In order to provide evidence that FAST did cross black aurora at the time that black aurora was observed in the cameras, the electron energy flux at 110 km is used as a proxy for optical emission.

[23] *Stenbaek-Nielsen et al.* [1998] and *Hallinan et al.* [2001] have shown excellent agreement between electron energy flux and the brightness of the broadband (white) optical emissions observed in the zenith of the all-sky and narrow-field TV cameras. Thus, for most auroral geometries, any significant (>50%), "thin" (<6 km at $\sim$110 km) and steep decrease in a uniform, sufficiently intense (>1 erg cm^{-2} s^{-1} at $\sim$110 km) downgoing electron energy flux measured by the instruments on board FAST is a good candidate for optical black aurora, provided that no further pitch angle scattering nor parallel acceleration occurs between FAST and the ionosphere. Thus finding black aurora in electron data is a matter of having sufficient time resolution in the electron energy flux to resolve the widths of black aurora as well as being able to correctly map the electrons from FAST altitudes into the collision-dominated ionosphere.

[24] Figure 3 shows two sharp decreases in the electron energy flux when electrons were being sampled every 79 ms. These energy flux decreases were measured when FAST's footprint was far from the magnetic zenith and outside the field of view of the narrow-field camera, but they occurred at the same time as black aurora was seen in the narrow-field camera.

[25] The percent difference of the energy flux from the average energy flux for the 25 s of data was calculated and is shown on the right side scale of the plots in Figure 3. At 0849:30 UT, labeled "black aurora 1", there is a 50% decrease in the electron energy flux and at 0851:07 UT, labeled "black aurora 2," the decrease is $\sim$60%, and in both of these cases, the decrease in energy flux has steep gradients representing a good contrast between the brightness and black aurora. FAST crosses these energy flux depletions in $\sim$1 s, which gives a width of 3 km not accounting for oblique crossings nor the finite drift speeds of the forms. This inferred width is within the observed widths ($\leq$6.5 km) and drift speeds ($\leq$1.7 km s^{-1}) of the black aurora in the narrow-field cameras, as discussed in section 3.1. The electron energy flux in Figure 3 is suffi-

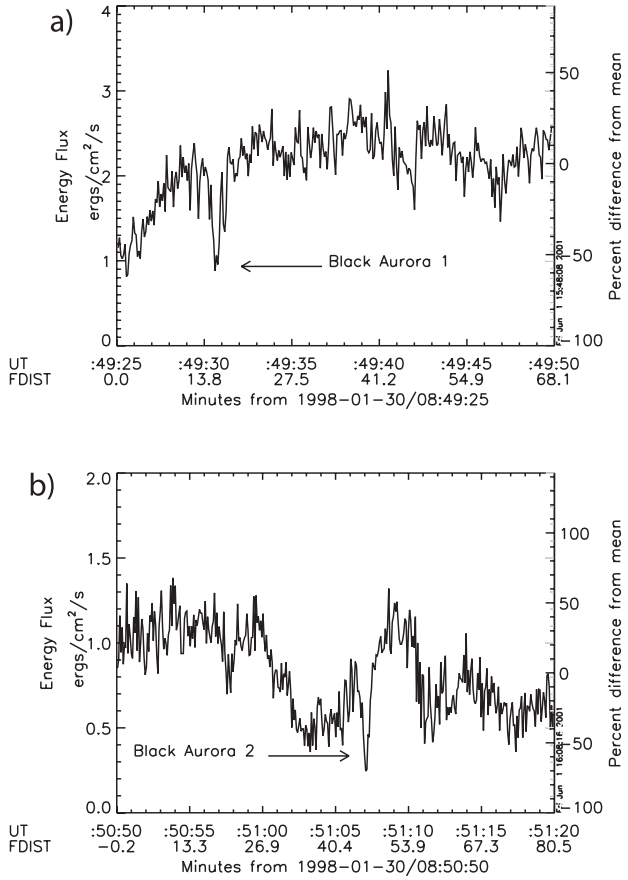

Figure 3. Electron burst data of depletion in energy flux mapped to 110 km.

ciently similar to depletions observed in optical black aurora that we are confident that this decrease in energy flux represents a magnetic conjunction between FAST and optical black aurora.

[26] The two short energy flux decreases detected by FAST and shown in Figure 3 are both due to decreases of the differential energy flux in the downward loss cone at high energies (>2 keV). In Figure 4 (top) the differential energy flux is shown as a function of energy and pitch angle for four different times: (1) at 0849:30.05 UT, adjacent to black aurora electron spectra; (2) at 0849:30.6 UT during a pass through black aurora (black aurora 1); (3) at 0851:07.397 UT adjacent to the second black aurora spectra, and (4) at 0851:07.125 UT during another pass through black aurora (black aurora 2).

[27] The differential energy flux at pitch angles of 0° (0 ± 22°) marked in green and 90° (90 ± 22°) marked in red are also shown in Figure 4 (bottom) to better contrast the energy fluxes of the mirroring versus precipitating fluxes. In the regions adjacent to the black aurora (0849:30.05 and 0851:07.397 UT) the downward differential electron energy fluxes at 0 ± 90° are "isotropic" at all energies greater than 800 eV creating a single loss cone (SLC) distribution. In the regions of inferred black aurora (0849:30 and 0851:07.125 UT) the electron differential energy fluxes are depleted in the precipitating loss cone, i.e., source cone (0 ± 22°), at energies greater than 2 keV. We will refer to this type of differential energy flux as a partial-double loss cone (PDLC) throughout the rest of the paper. This PDLC is responsible for the decrease in energy flux shown in Figure 3 and thus for the decrease in emissions in optical black aurora.

[28] The SLC adjacent to the black auroral PDLC in Figure 4 have the same differential energy fluxes in the mirroring electron population (θ = 90°). In fact, these fluxes are different only in the precipitating fluxes (θ = 0°). This implies that electrons were not accelerated or decelerated differently in the black aurora (region of the PDLC) than in the diffuse aurora (region of the SLC). Thus the mechanism for creating the "black" in black aurora acts only on the precipitating fluxes and at energies greater than ~2 keV.

4.1. A Multicase Study of Electron Spectra

[29] Six nights of FAST/aircraft conjunctions were chosen for comparisons with the night of the black aurora. All conjunctions, including that with the black aurora, were in the premidnight sector of the auroral oval (20–22 MLT). The

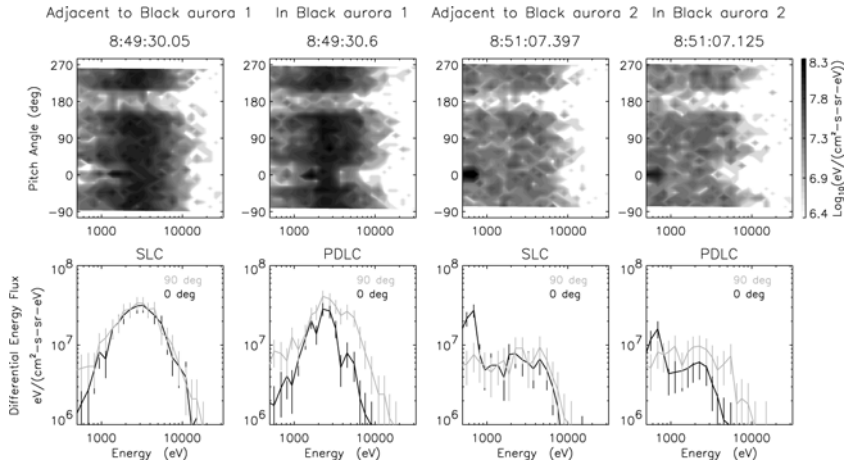

Figure 4. Electron differential energy fluxes as a function of pitch angle and energy at selected times (top). Electron differential energy fluxes as a function of energy plotted for pitch angles from −22° to 22° (marked as "0 deg") and for pitch angles from 68° to 112° (marked as "90 deg"). See color version of this figure at back of this issue.

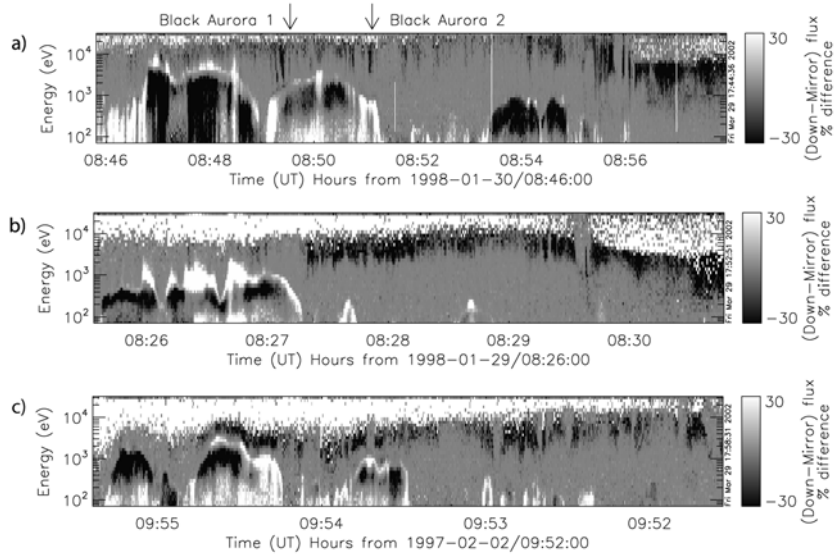

Figure 5. The anisotropy of the downgoing electrons at FAST altitudes as a function of energy and time across the auroral oval for three different crossings. Blue/black regions above 2 keV indicate partial double loss cones, green regions indicate single loss cones, and red regions indicate accelerated electrons. See the text for details. See color version of this figure at back of this issue.

auroral forms near the magnetic zenith of the all-sky camera included: multiple arcs (three nights), a single arc (one night), diffuse aurora with pulsating aurora (one night), and ray bundles (one night).

[30] On 30 January 1998 (black aurora observed), single loss cones (SLCs) were measured more often than partial double loss cones (PDLCs). However, on the other six nights studied, PDLCs were measured more often than SLCs. Displaying the change from isotropy to anisotropy as a function of energy and time in the downgoing electron differential energy fluxes across the entire auroral oval demonstrates the spatial distribution of the PDLC and SLC electron signatures. In order to show such an anisotropy time series, we have calculated the percent difference, $PD_{dm}(E, t)$, of the mirroring differential electron energy fluxes ($\theta = 90 \pm 22°$), $JE_m(E, t)$, from the precipitating energy energy fluxes ($\theta = 0 \pm 22°$), $JE_d(E, t)$, at every energy and time:

$$PD_{dm}(E,t) = \frac{JE_d(E,t) - JE_m(E,t)}{JE_m(E,t)} * 100\% \qquad (1)$$

This percent difference, $PD_{dm}(E, t)$, is shown in Figure 5 for three nights when the following optical signatures were seen in the all-sky camera: (1) diffuse and black aurora (30 January 1998 from 0848 to 0851 UT), (2) multiple arcs (29 January 1998 from 0825 to 0828 UT), and (3) diffuse and pulsating aurora (2 February 1997 from 0951 to 0954 UT).

[31] When the mirroring fluxes are the same as the precipitating fluxes, the color scale is green (0% difference). Thus the time-energy regions that are green represent a downward isotropic distribution, which is most often an SLC. The black regions indicate a greater than 30% difference between mirroring and precipitating fluxes. The black regions at high energies are the regions that represent PDLCs. The black regions at lower energies are indicative of a parallel acceleration above FAST. When the precipitating fluxes are larger than the mirroring fluxes, also an indication of parallel acceleration, the color scale is red (<−30% difference). The white regions at high energies are regions where the mirroring flux was below the detection threshold. The black aurora PDLCs have been marked with arrows, although the survey mode electron data makes these narrow regions difficult to discern. The larger regions of PDLCs just to the left of black aurora 1 is too large to meet our criteria for optical black aurora.

[32] As can be seen in Figure 5 (top) on the night when black aurora was observed (30 January 1998), PDLCs were located in narrow spatial regions (black surrounded by green at energies greater than ~1 keV) and were less common than the SLC (green regions at energies greater than 1 keV). During the night of 29 January 1998 FAST traversed multiple arcs from 0826–0827:30 UT and the anisotropy spectra (PD_{dm}) at these times is red with black at lower energies implying electron acceleration above FAST. From 0827:30 to 0840 UT the equatorward section of the auroral oval was characterized by PDLCs (colored black at higher energies between the green and white), as shown in Figure 5 (middle). The prevalence of the black regions over a wide range of times indicates that the PDLC distribution was most common, especially in the central plasma sheet (CPS) [*Winningham et al.*, 1975], i.e., equatorward region of the auroral oval where one would expect to observe diffuse aurora. In fact, the SLCs are only present in association with the accelerated spectra (from 0826 to 0827:20 UT) and for short times in the equatorward oval, around 0829:00 UT and 0829:40 UT.

[33] During the night of pulsating aurora on 2 February 1997, there was structure in the diffuse aurora. This structure is associated with smaller spatial regions of SLC distributions surrounded by the PDLCs, as shown in Figure 5 (bottom). In this case, the spatial regions of

continuous PDLC distributions are too broad to be called black aurora but the regions are not as large as observed in the anisotropy spectra of 29 January 1998 shown in the middle panel of Figure 5. The anisotropy spectra for the four nights not shown here indicate that PDLCs are the most common spectra in the central plasma sheet (CPS).

[34] When comparing properties of the CPS electrons of the seven nights studied, a clear difference was found in the temperature of the electrons on the night when black aurora was observed. On this night, the average temperature of the CPS electrons was 1.8 ± 0.5 keV. The average CPS electron temperature of the other six nights combined was 1.0 ± 0.2 keV. Of all the nights the second hottest electron plasma sheet occurred when pulsating aurora was observed by the TV all-sky cameras on 2 February 1997 with a temperature of 1.2 ± 0.3 keV. Black aurora is also seen during periods of pulsating aurora. Thus it seems that the temperature of the plasma sheet plays an important role in producing large regions of SLC signatures and in the occurrence of black aurora in particular.

[35] Because of the strong evidence in observations and theories that positive space charge and downward electric fields are associated with black auroral curls, we examined the seven nights discussed above to look for signatures of large differential fluxes of upward moving electrons, diverging shocks, and downward currents. All seven of the nights had such signatures on the equatorward boundary of the auroral oval and three nights had such signatures on the poleward boundary. However, electron energy flux signatures of black aurora in these regions were only found on the night when black aurora was observed in the TV cameras. The upward electron beam and downward current for this black aurora night can be seen in panels 2 and 7 of Figure 2 in the region marked with an E. In this single case when there were both electron depletions at high energies and field signatures of black curls on the equatorward boundary, the correlation between the PDLC electron signatures and the fields and the electrons was more random than causal.

5. Discussion

[36] The electron energy flux measurements associated with black aurora, as shown in Figure 2, demonstrated large decreases in the precipitating electrons at energies above ~2 keV, producing PDLC differential energy fluxes. Such signatures are suggestive of narrow plasma sheet regions in which there are reductions in pitch angle diffusion at the higher energies. These narrow regions in which the loss cone was partially empty were surrounded by broad spatial regions of pitch angle diffusion at all measured energies, producing the SLC electron signatures. In agreement with these measurements, *Kimball and Hallinan* [1998b] showed that when pulsating aurora overlaps regions of black aurora, the pulsations often add to the intensity in the black aurora more than in the surrounding diffuse aurora (veiling). This veiling was interpreted as an indication that the loss cone was not filled to capacity in the black aurora and that the pulsations fill this loss cone. One possible explanation of the black aurora and the diffuse aurora surrounding the black aurora is that the pitch angle diffusion causing the SLCs and PDLCs is initiated by two types of wave-particle interactions in the plasma sheet, at least one of which is energy sensitive.

[37] Strong pitch angle scattering occurs when plasma waves diffuse particles across the loss cone in less than a quarter of a bounce period, creating isotropic pitch angle distributions at low altitudes [*Kennel and Engelmann*, 1969]. There are two types of waves in the plasma sheet that can strongly scatter electrons at the measured energies into the atmospheric loss cone: oblique whistler mode waves [e.g., *Inan et al.*, 1992; *Johnstone et al.*, 1993; *Villalón and Burke*, 1995] and electrostatic electron cyclotron harmonic (ECH) waves [e.g., *Kennel and Engelmann*, 1969; *Lyons*, 1974; *Horne and Thorne*, 2000]. Whether the ECH wave power measured in the plasma sheet is sufficient to produce diffuse aurora at energies greater than ~1 keV and whether whistler waves can, in fact, scatter such low energy electrons (<10 keV) have been matters of debate [*Hultqvist et al.*, 1999, p. 122, and references therein]. More recently, it has been shown that both types of waves are important in scattering the hot plasma sheet electrons into the loss cone during periods of auroral activity (plasma sheet injections) [*Meredith et al.*, 1999, 2000; *Horne and Thorne*, 2000].

[38] *Inan et al.* [1992] modeled the effect of strongly scattering electrons into the loss cone by obliquely propagating upper band (UB) and lower band (LB) whistler mode chorus waves. From these modeling results they suggested that the high-energy (~10–50 keV) electrons often related to pulsating aurora are scattered by the LB chorus waves, that the intermediate-energy (~1–10 keV) electrons associated with diffuse aurora are scattered by the UB chorus and that the low-energy (<1 keV) precipitating electrons are secondary electrons backscattered from the conjugate atmosphere. It is also possible that UB chorus that propagates near the resonance cone can strongly scatter electrons with energies less than 1 keV into the loss cone [e.g., *Inan et al.*, 1992; *Johnstone et al.*, 1993; *Villalón and Burke*, 1995]. The modeling efforts of *Inan et al.* [1992] and *Villalón and Burke* [1995] are consistent with the above mentioned optical observations of *Kimball and Hallinan* [1998b].

[39] Expanding on the above suggestion by *Inan et al.* [1992], we propose that the SLCs are due to oblique UB whistler mode chorus waves and that the PDLCs are caused by a suppression of scattering by UB chorus waves in narrow regions in the plasma sheet. Since the backscattered electron fluxes measured by FAST did not match the precipitating fluxes below 2 keV, as shown in Figure 2, there must be another mechanism responsible for the low-energy precipitating electrons. Measurements and theory show that ECH waves can be effective in precipitating electrons with energies from ~0.5–2 keV [*Belmont*, 1983; *Horne and Thorne*, 2000; *Meredith et al.*, 2000]. We suggest that these waves cause the precipitation at lower energies in all the plasma sheet regions.

[40] In the multicase study of electron spectra discussed in section 4.1, it was shown that for most diffuse aurora in the premidnight auroral zone (20–22 MLT) the PDLC is common. This implies that strong pitch angle scattering of the hot plasma sheet electrons at all energies is rare. This is in agreement with several studies of diffuse aurora [e.g., *Fairfield and Viñas*, 1984; *Schumaker et al.*, 1989; *Chen*

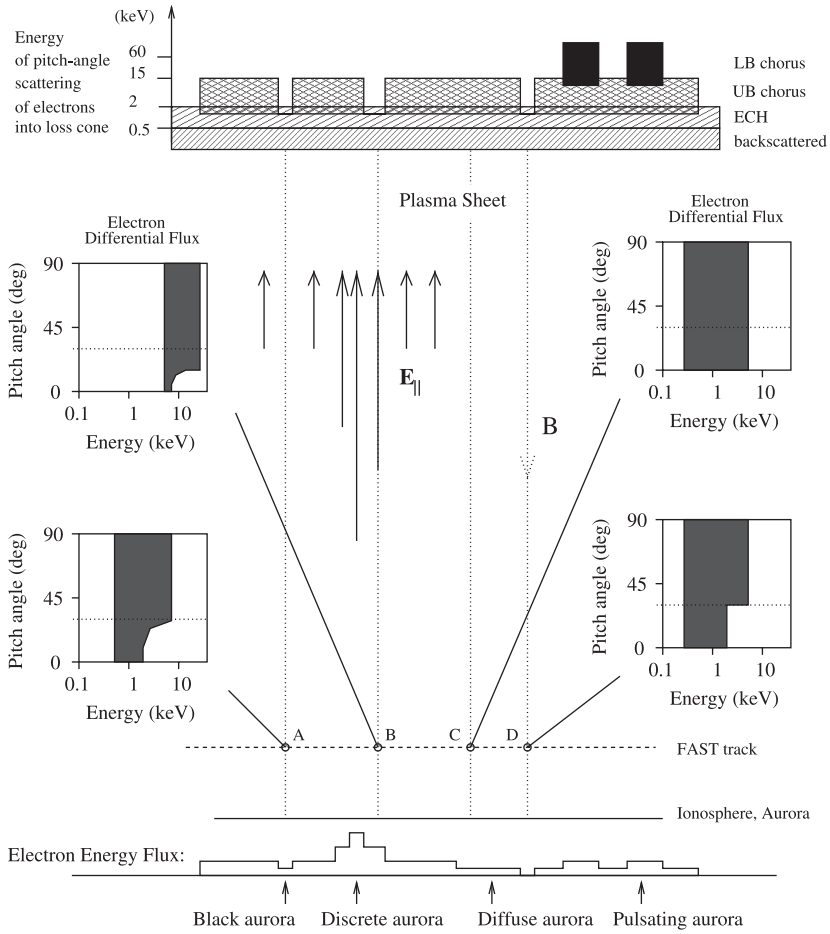

Figure 6. A cartoon of the mechanisms discussed in the text regarding pitch angle scattering and parallel electron acceleration in relation to black, discrete, diffuse, and pulsating aurora. These types of aurora are typical of what optical cameras observe in the recovery phase of substorms. See text for details.

and Schulz, 2001]. The lack of pitch angle scattering at intermediate energies is also in agreement with our suggestion regarding ECH and chorus waves because these waves are both associated with substorms and because whistler mode waves in the near-Earth plasma sheet are rarely observed at magnetic local times from 20–22 MLT (from which our data were taken) [*Tsurutani and Smith*, 1974; *Parrot and Gaye*, 1994; *Meredith et al.*, 1999, 2000].

[41] Black arcs, arc segments, and curls were all located in a region in which there was an inferred small potential drop above FAST altitudes that slowly varied in time. As the strength of the potential drop increased, the energy of the peak in the precipitating electron energy flux became larger than the plasma temperature. Consequently, the black aurora disappeared. It then reappeared only after the potential drop above FAST decreased to below the plasma temperature. A cartoon of the inferred physical mechanisms important to these types of auroral observations associated with black aurora is shown in Figure 6.

[42] In this cartoon the energy at which the pitch angle scattering of electrons into the loss cone is efficient is shown along with the mechanisms proposed to be responsible for the scattering. Parallel electric fields are shown as arrows between the plasma sheet and the altitude of the FAST trajectory. The electron energy flux is shown at the bottom of the plot along with the associated auroral forms. The differential electron fluxes greater than 2×10^6 eV/(cm^2 s^{-1} sr^{-1} eV^{-1}) are shown as a shaded regions in energy pitch angle space in four different auroral regions. The source cone in these four diagrams is indicated with dashed lines around 30°.

[43] The region marked A (Figure 6) is characterized by a lack of pitch angle scattering at higher energies in the plasma sheet with a small upward electric field in the acceleration region. The differential energy flux shows a PDLC that has gone through a small potential drop. Note that the backscattered electrons are not included in the differential energy flux diagrams. In region A, the electric field increases the chance of ground-based TV cameras observing optical black aurora. The region marked B is also characterized by a lack of pitch angle scattering but because the electric fields are much larger, the differential energy flux in the loss cone increases as the energy of the electrons increase. Discrete auroral features can form as a consequence of this large acceleration in regions both with and without pitch angle scattering at high energies. In region C, scattering at all energies in the plasma sheet produces a SLC differential energy flux to create diffuse aurora. The energy flux in this

region might not be great enough to produce emissions brighter than the airglow. The region D is also a region described by a lack of pitch angle scattering at the higher energies and produces black aurora but without the effects of a parallel electric field. The black aurora in this region is surrounded by diffuse aurora that may be too weak to observe optically. Pulsating aurora is shown on the right side of the Figure 6 as being caused by LB chorus waves scattering high-energy electrons into the loss cone.

[44] Black auroral forms are often found on the boundary between diffuse and discrete aurora as well as in aurora that changes in time between diffuse and discrete [*Oguti*, 1975; *Kimball and Hallinan*, 1998a, 1998b]. From our study we have shown that black aurora occurs equatorward of the boundary plasma sheet (BPS) associated with the structured, accelerated electrons that produce the discrete aurora and poleward of the innermost central plasma sheet (CPS) associated with hot plasma sheet electrons that produce the diffuse aurora [*Winningham et al.*, 1975]. In this region the electric potential varied in time, changing the type of aurora from diffuse to discrete to diffuse. Further studies of this boundary using low-altitude satellites such as FAST as well as high-altitude magnetospheric satellites should help to understand the origins of optical black auroral forms.

5.1. Black Aurora and Positive Space Charge

[45] FAST has measured upgoing electrons in downward field-aligned current regions with diverging DC electric fields [*McFadden et al.*, 1999, and references therein]. These regions are often proposed to be the regions of black aurora following the suggestion by *Marklund et al.* [1994, 1997], as discussed in section 1. In general, the prevalence of clockwise vortex streets (curls) in black aurora indicates that the mechanism for causing black aurora is associated with positive space charge. Diverging electric fields (positive space charge) are consistent with our observation of curls in a black arc located in the magnetic zenith, as shown in Figure 1. Since this black arc appeared only three minutes prior to the FAST conjunction and since the all-sky auroral configuration did not change radically in this time, the FAST electron data in Figure 2 indicates that the black curl was located in the middle of the auroral oval between the CPS and the BPS.

[46] It is likely that positive space charge was also associated with the two regions of black aurora studied in this paper but that it was too small to trigger the Kelvin-Helmholtz instability and too small to be detected by the FAST electric fields experiment. If positive space charge and the suppression of whistler waves are both aspects of black aurora, then studying the relationship between these two mechanisms will be important. To better understand black auroral diverging electric fields, future studies should examine diverging electric fields associated with sharp, small electron energy flux decreases in the middle of the auroral oval. No such simultaneous signatures were observed in any of the nights studied here.

[47] The more common diverging electric fields with downward currents and upward electron beams are located on the boundaries of the auroral oval (section 4.1). These signatures cannot be, in general, associated with optical black aurora. Previous FAST studies have shown that upward electron beams in downward current regions are often (~71% of the time) observed in the premidnight auroral oval when the ionosphere is in darkness [e.g., *Carlson et al.*, 1998; *Peria et al.*, 2000; *Elphic et al.*, 2000]. These regions measured by FAST are also associated with positive charge [e.g., *Carlson et al.*, 1998] and are similar to the regions described by *Marklund et al.* [1994, 1997]. Statistics show that both diverging shocks and electron beams occur at low altitudes in regions with the ionospheric footprint in darkness [*Marklund et al.*, 1997; *Peria et al.*, 2000; *Elphic et al.*, 2000]. However, in these boundary regions, there is often not enough precipitating electron energy flux to produce the emissions surrounding the upward electron beams needed to create optical black aurora, as can be seen in Figure 1 of *Elphic et al.* [1998] and Figure 5 of *Stenbaek-Nielsen et al.* [1998] or, the regions of upward electron beams are too wide to qualify as optical black aurora, as seen in Figure 1 of *Carlson et al.* [1998]. Following *Carlson et al.* [1998], we suggest that these signatures be referred to as inverse aurora rather than black aurora.

6. Summary

[48] In our study of black aurora from FAST plasma and fields measurements and optical TV observations we have found that:

1. Black aurora occurred in narrow spatial regions of partial double loss cones (PDLCs) sandwiched between broad regions of single loss cones (SLCs).
2. The SLC-PDLC-SLC electron signature of black aurora can be explained by using a combination of electron cyclotron harmonic (ECH) and whistler mode, upper band chorus waves, and the suppression of the chorus waves in the region of the black aurora PDLC.
3. In the central plasma sheet region of the premidnight auroral oval, PDLCs are common implying that strong pitch angle scattering at all energies is not common in this region.
4. Black aurora occurred in a region of small earthward electron acceleration.
5. The measured electric fields were small with no evidence of diverging shocks at FAST nor of parallel deceleration of the electrons above the satellite, nor of significant fluxes of upward directed electrons near black aurora.
6. Upward electrons and diverging shocks were most common on the equatorward edge of the auroral oval. In this region, there was only evidence for black aurora in the electron energy flux during the night when black aurora was observed in the TV cameras.

[49] **Acknowledgments.** We would like to thank R. E. Ergun for providing the electric fields data and R. P. Strangeway for providing the magnetic fields data. One of us, L. M. Peticolas, would like to thank D. Lummerzheim for providing his transport code, C. C. Chaston for helpful discussions regarding the manuscript as well as the FAST data, and M. J. Heavner for his comments on the manuscript. This paper was written under NASA grant NAG5-3596.

[50] Hiroshi Matsumoto thanks G. Ganguli and another referee for their assistance in evaluating this paper.

References

Belmont, G., Are equatorial electron cyclotron waves responsible for diffuse auroral electron precipitation?, *J. Geophys. Res.*, *88*, 9163, 1983.

Carlson, C. W., et al., FAST observations in the downward auroral current region: Energetic upgoing electron beams, parallel potential drops and ion heating, *Geophys. Res. Lett.*, *25*, 2017, 1998.

Carlson, C. W., J. P. McFadden, P. Turin, D. W. Curtis, and A. Magoncelli, The electron and ion plasma experiment for FAST, *Space Sci. Rev.*, *98*, 33, 2001.

Chen, M. W., and M. Schulz, Simulations of storm time diffuse aurora with plasmasheet electrons in strong pitch angle difffusion, *J. Geophys. Res.*, *106*, 1873, 2001.

Davis, T. N., Observed microstructure of auroral forms, *J. Geomagn. Geoelectr.*, *30*, 371, 1978.

Elphic, R., J. Bonnell, R. Strangeway, C. Carlson, M. Temerin, J. McFadden, R. Ergun, and W. Peria, Fast observations of upward accelerated electron beams and the downward field-aligned current region, in *Magnetospheric Current Systems, Geophys. Monogr. Ser.*, vol. 118, edited by S.-I. Ohtani et al., p., AGU, Washington, D. C., 2000.

Elphic, R. C., et al., The auroral current circuit and field-aligned currents observed by FAST, *Geophys. Res. Lett.*, *25*, 2033, 1998.

Elphic, R. C., J. D. Means, R. C. Snare, R. J. Strangeway, L. Kapko, and R. E. Ergun, Magnetic field instruments for the Fast Auroral SnapshoT explorer, *Space Sci. Rev.*, *98*, 151, 2001.

Ergun, R. E., et al., Fast satellite observations of large-amplitude solitary structures, *Geophys. Res. Lett.*, *25*, 2041, 1998.

Ergun, R. E., C. W. Carlson, J. P. McFadden, F. S. Mozer, and R. J. Strangeway, Parallel electric fields in discrete arcs, *J. Geophys. Res.*, *27*, 4053, 2000.

Ergun, R. E., C. W. Carlson, F. S. Mozer, G. T. Delory, M. Temerin, J. P. McFadden, D. Pankow, R. Abiad, P. Harvey, R. Wilkes, and H. Primbsch, The FAST satellite electric field and magnetic field instrument, *Space Sci. Rev.*, *98*, 67, 2001.

Fairfield, D. H., and A. F. Viñas, The inner edge of the plasma sheet and the diffuse aurora, *J. Geophys. Res.*, *89*, 841, 1984.

Hallinan, T. J., and T. N. Davis, Small-scale auroral arc distortions, *Planet. Space Sci.*, *18*, 1735, 1970.

Hallinan, T. J., J. Kimball, H. C. Stenbaek-Nielsen, K. Lynch, R. Arnoldy, J. Bonnell, and P. Kintner, Relation between optical emission, particles, electric fields and Alfven waves in a multiple rayed arc, *J. Geophys. Res.*, *106*, 15,445, 2001.

Hedin, A. E., Extension of the MSIS thermosphere model into the middle and lower atmosphere, *J. Geophys. Res.*, *96*, 1159, 1991.

Horne, R. B., and R. M. Thorne, Electron pitch angle diffusion by electrostatic electron cyclotron harmonic waves: The origin of pancake distributions, *J. Geophys. Res.*, *105*, 5391, 2000.

Hultqvist, B., M. Øieroset, G. Paschmann, and R. Treumann, Magnetospheric plasma sources and losses, *Space Sci. Rev.*, *88*, 1, 1999.

Inan, U. S., Y. T. Chiu, and G. T. Davidson, Whistler-mode chorus and morningside aurorae, *Geophys. Res. Lett.*, *19*, 653, 1992.

Johnson, J., and T. Chang, Nonlinear vortex structures with diverging electric fields and their relation to the balck aurora, *Geophys. Res. Lett.*, *22*, 1481, 1995.

Johnstone, A. D., D. M. Walton, R. Liu, and D. A. Hardy, Pitch angle diffusion of low-energy electrons by whistler mode waves, *J. Geophys. Res.*, *98*, 5959, 1993.

Kennel, C. F., and F. Engelmann, Velocity space diffusion from weak plasma turbulence in a magnetic field, *Phys. Fluids*, *9*, 2377, 1969.

Keskinen, M. J., and G. Ganguli, Simulation of dynamics and structure in the black aurora, *J. Geophys. Res.*, *101*, 26,995, 1996.

Kimball, J., and T. J. Hallinan, A morphological study of black vortex streets, *J. Geophys. Res.*, *103*, 14,683, 1998a.

Kimball, J., and T. J. Hallinan, Observations of black auroral patches and of their relationship to other types of aurora, *J. Geophys. Res.*, *103*, 14,671, 1998b.

Lummerzheim, D., and J. Lilensten, Electron transport and energy degradation in the ionosphere: Evaluation of the numerical solution, comparison with laboratory experiments and auroral observations, *Ann. Geophys.*, *12*, 1039, 1994.

Lyons, L. R., Electron diffusion driven by magnetospheric electrostatic waves, *J. Geophys. Res.*, *79*, 575, 1974.

Marklund, G., L. Blomberg, C. G. Falthammar, and P. A. Lindqvist, On intense diverging electric fields associated with black aurora, *Geophys. Res. Lett.*, *21*, 1859, 1994.

Marklund, G., T. Karlsson, and J. Clemmons, On low-altitude particle acceleration and intense electric fields and their relationship to black aurora, *J. Geophys. Res.*, *102*, 17,509, 1997.

McFadden, J. P., C. W. Carlson, and R. E. Ergun, Microstructure of the auroral acceleration region as observed by FAST, *J. Geophys. Res.*, *104*, 14,453, 1999.

Meredith, N. P., A. D. Johnstone, S. Szita, R. B. Horne, and R. R. Anderson, Pancake electron distributions in the outer radiation belts, *J. Geophys. Res.*, *104*, 12,431, 1999.

Meredith, N. P., R. B. Horne, A. D. Johnstone, and R. R. Anderson, The temporal evolution of electron distributions and associated wave activity following substorm injections in the inner magnetosphere, *J. Geophys. Res.*, *105*, 12,907, 2000.

Oguti, T., Metamorphoses of aurora, *Mem. Natl. Inst. Polar Res. Spec. Issue Jpn.*, *12*, 101, 1975.

Parrot, M., and C. A. Gaye, A statistical survey of ELF waves in a geostationary orbit, *Geophys. Res. Lett*, *21*, 2463, 1994.

Peria, W. J., C. W. Carlson, R. E. Ergun, J. P. McFadden, J. Bonnell, R. C. Elphic, and R. J. Strangeway, Characteristics of field-aligned currents near the auroral acceleration region: FAST observations, in *Magnetospheric Current Systems, Geophys. Monog. Ser.*, vol. 118, edited by S.-I. Ohtani et al., p., AGU, Washington, D. C., 2000.

Royrvik, O., *Pulsating aurora: Local and global morphology*, Ph.D. thesis, Univ. of Alaska, Fairbanks, 1976.

Schoute-Vanneck, H., M. W. Scourfield, and E. Nielsen, Drifting black aurorae?, *J. Geophys. Res.*, *95*, 241, 1990.

Schumaker, T. L., M. S. Gussenhoven, D. A. Hardy, and R. L. Carovillano, The relationship between diffuse auroral and plasma sheet electron distributions near local midnight, *J. Geophys. Res.*, *94*, 10,061, 1989.

Stenbaek-Nielsen, H. C., T. J. Hallinan, D. L. Osborne, J. Kimball, C. Chaston, J. McFadden, G. Delory, M. Temerin, and C. W. Carlson, Aircraft observations conjugate to FAST: Auroral arc thicknesses, *Geophys. Res. Lett.*, *25*, 2073, 1998.

Trondsen, T. S., and L. L. Cogger, High-resolution television observations of black aurora, *J. Geophys. Res.*, *102*, 363, 1997.

Trondsen, T. S., and L. L. Cogger, A survey of small-scale spatially periodic distortions of auroral forms, *J. Geophys. Res.*, *103*, 9405, 1998.

Tsurutani, B. T., and E. J. Smith, Postmidnight chorus: A substorm phenomenon, *J. Geophys. Res.*, *1974*, 118, 1974.

Villalón, E., and W. J. Burke, Pitch angle scattering of diffuse auroral electrons by whistler mode waves, *J. Geophys. Res.*, *100*, 19,361, 1995.

Vogt, J., H. U. Frey, G. Haerendel, H. Höfner, and J. L. Semeter, Shear velocity profiles associated with auroral curls, *J. Geophys. Res.*, *104*, 17,277, 1999.

Winningham, J. D., F. Yasuhara, S. I. Akasofu, and W. J. Heikkila, The latitudinal morphology of 10-eV to 10-keV electron fluxes during magnetically quiet and disturbed times at 2100–0300 MLT sector, *J. Geophys. Res.*, *80*, 3148, 1975.

J. W. Bonnell, C. W. Carlson, and L. M. Peticolas, Berkeley Space Science Laboratory, University of California, Centennial Drive at Grizzly Peak Blvd, Berkeley, CA 94720-7450, USA. (LMP@ssl.berkeley.edu)

T. J. Hallinan and H. C. Stenbaek-Nielsen, Geophysical Institute, University of Alaska Fairbanks, 903 Koyukuk Drive, P.O. Box 757320, Fairbanks, AK 99775, USA.

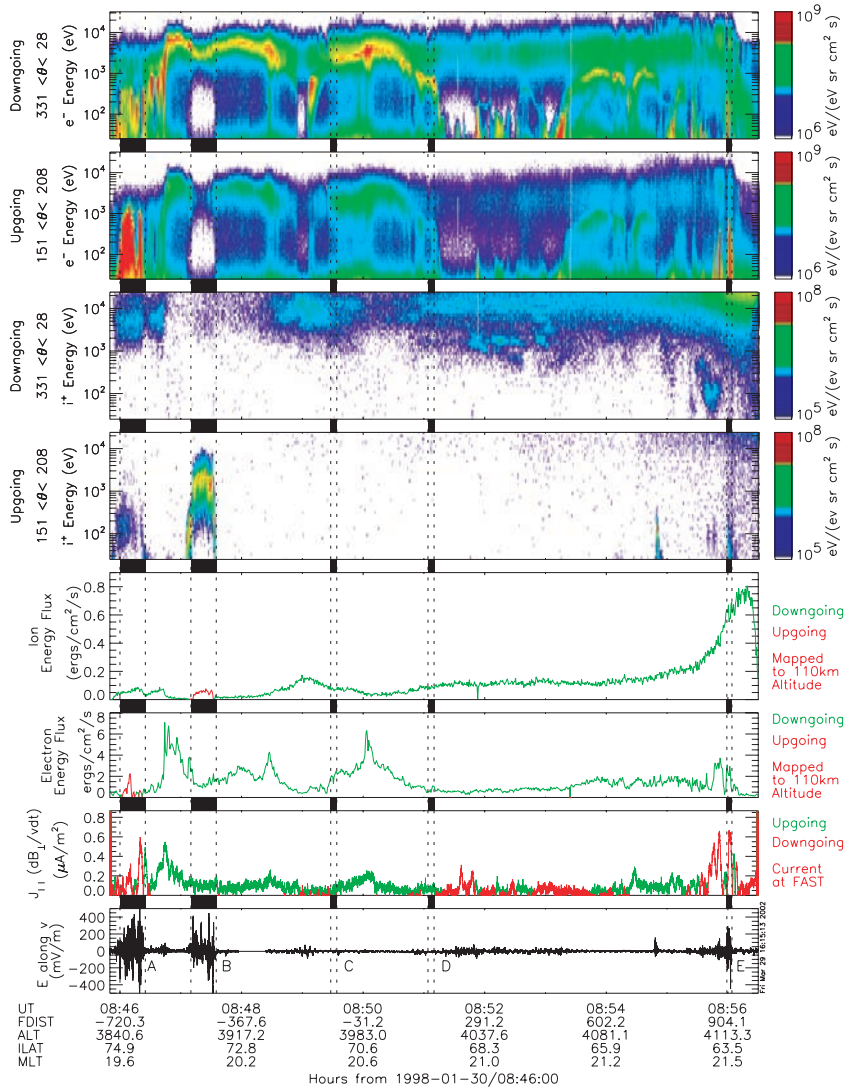

Figure 2. Particle and field measurements for FAST orbit 5700. See text for details.

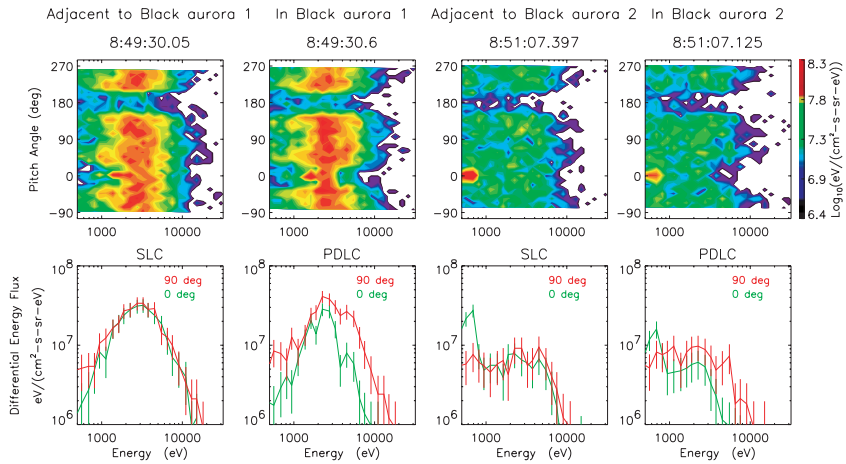

Figure 4. Electron differential energy fluxes as a function of pitch angle and energy at selected times (top). Electron differential energy fluxes as a function of energy plotted for pitch angles from −22° to 22° (marked as "0 deg") and for pitch angles from 68° to 112° (marked as "90 deg").

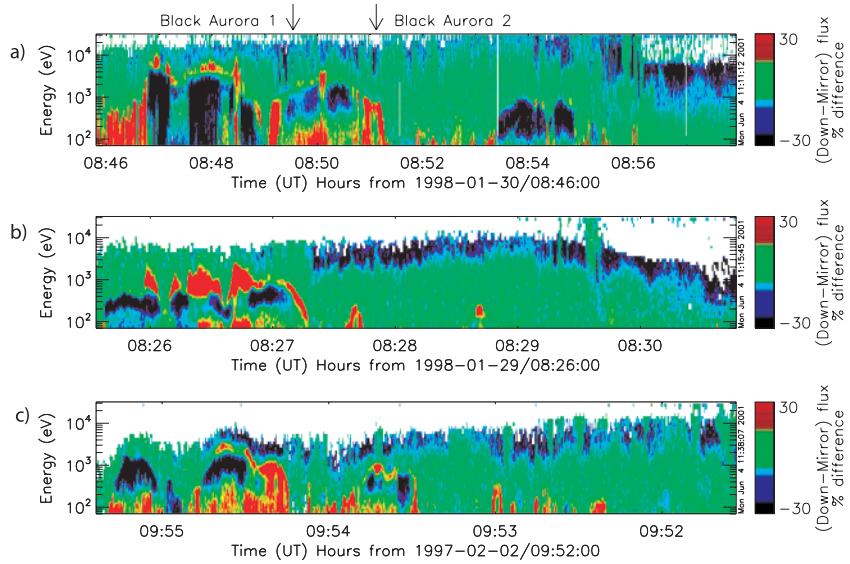

Figure 5. The anisotropy of the downgoing electrons at FAST altitudes as a function of energy and time across the auroral oval for three different crossings. Blue/black regions above 2 keV indicate partial double loss cones, green regions indicate single loss cones, and red regions indicate accelerated electrons. See the text for details.